

Optimisation of Spectral Wavelets for Persistence-based Graph Classification

KA MAN YIM¹ AND JACOB LEYGONIE²

Mathematical Institute, University of Oxford

ABSTRACT. A graph's spectral wavelet signature determines a filtration, and consequently an associated set of extended persistence diagrams. We propose a framework that optimises the choice of wavelet for a dataset of graphs, such that their associated persistence diagrams capture features of the graphs that are best suited to a given data science problem. Since the spectral wavelet signature of a graph is derived from its Laplacian, our framework encodes geometric properties of graphs in their associated persistence diagrams and can be applied to graphs without a priori vertex features. We demonstrate how our framework can be coupled with different persistence diagram vectorisation methods for various supervised and unsupervised learning problems, such as graph classification and finding persistence maximising filtrations, respectively. To provide the underlying theoretical foundations, we extend the differentiability result for ordinary persistent homology to extended persistent homology.

1. Introduction

1.1. Background. Graph classification is a challenging problem in machine learning. Unlike data represented in Euclidean space, there is no easily computable notion of distance or similarity between graphs. As such, graph classification requires techniques that lie beyond mainstream machine learning techniques focused on Euclidean data. Much research has been conducted on methods such as graph neural networks (GNNs) [Xu+19] and graph kernels [Vis+10; She+09] that embed graphs in Euclidean space in a consistent manner.

Recently, *persistent homology* [ZC05; EH08] has been applied as a feature map that explicitly represents topological and geometric features of a graph as a set of *persistence diagrams* (a.k.a. *barcodes*). In the context of our discussion, the persistent homology of a graph $G = (V, E)$ depends on a vertex function $f : V \rightarrow \mathbb{R}$. In the case where a vertex function is not given with the data, several schemes have been proposed in the literature to assign vertex functions to graphs in a consistent way. For example, vertex functions can be constructed using local geometric descriptions of vertex neighbourhoods, such as discrete curvature [ZW19] and heat kernel signatures [Car+20b].

E-mail address: ¹yim@maths.ox.ac.uk, ²leygonie@maths.ox.ac.uk.

However, it is often difficult to know *a priori* whether a heuristic vertex assignment scheme will perform well in addressing different data science problems. For a single graph, we can optimise the vertex function over $|V|$ many degrees of freedom in \mathbb{R}^V . In recent years, there have been many other examples of persistence optimisation in data science applications. The first two examples of persistence optimisation are the computation of Fréchet mean of barcodes using gradients on Alexandrov spaces [Tur+14], and that of point cloud inference [GHO16], where a point cloud is optimised so that its barcode fits a target fixed barcode. The latter is an instance of topological inverse problems (see Oudot and Solomon [OS18] for a recent overview of such). Another inverse problem is that of surface reconstruction [Brü+20]. Besides, in the context of shape matching [PSO18], persistence optimisation is used in order to learn an adequate function between shapes. Finally, there are also many recent applications of persistence optimisation in Machine Learning, such as the incorporation of topological information in Generative Modelling [Moo+19; Hof+19b; Gab+20] or in Image Segmentation [Hu+19; Clo+19], the design of topological losses for Regularization in supervised learning [Che+19] or for dimension reduction [Kac20].

Each of these applications can be thought of as minimising a certain *loss* function over a manifold \mathcal{M} of parameters:

$$\min_{\theta \in \mathcal{M}} \mathcal{L}(\theta),$$

where $\mathcal{L} : \mathcal{M} \rightarrow \mathbf{Bar}^N \rightarrow \mathbb{R}$ factors through the space \mathbf{Bar}^N of N -tuples of barcodes. The aim is to find the parameter θ that best fits the application at hand. Gradient descent is a very popular approach in minimisation, but it requires the ability to differentiate the loss function. In fact, Leygonie, Oudot, and Tillmann [LOT19] provide notions of differentiability for maps in and out \mathbf{Bar} that are compatible with smooth calculus, and show that the loss functions \mathcal{L} corresponding to the applications cited in the above paragraph are generically differentiable. The use of (stochastic) gradient descent is further legitimised by Carriere et al. [Car+20a], where convergence guarantees on persistence optimisation problems are devised, using a recent study of stratified non-smooth optimisation problems [Dav+20]. In practice, the minimisation of \mathcal{L} can be unstable due to its non-convexity and partial non-differentiability. Some research has been conducted in order to smooth and regularise the optimisation procedure [SWB20; CD20].

In a supervised learning setting, we want to optimise our vertex function assignment scheme over many individual graphs in a dataset. Since graphs may not share the same vertex set and come in different sizes, optimising over the $|V|$ degrees of freedom of any one graph is not conducive to learning a vertex function assignment scheme that can generalise to another graph. The degrees of freedom in any practical vertex assignment scheme should be independent of the number of vertices of a graph. However, a framework for parametrising and optimising the vertex functions of many graphs over a common parameter space \mathcal{M} is not immediately apparent. An example can be found in Hofer et al. [Hof+19a] who proposes a graph persistence optimisation framework based on graph isomorphism networks (GINs) [Xu+19], a neural network which maps vertex degrees to a new vertex function. Here, we propose an optimisable vertex assignment scheme without the input of an initial vertex function to initialise the optimisation process.

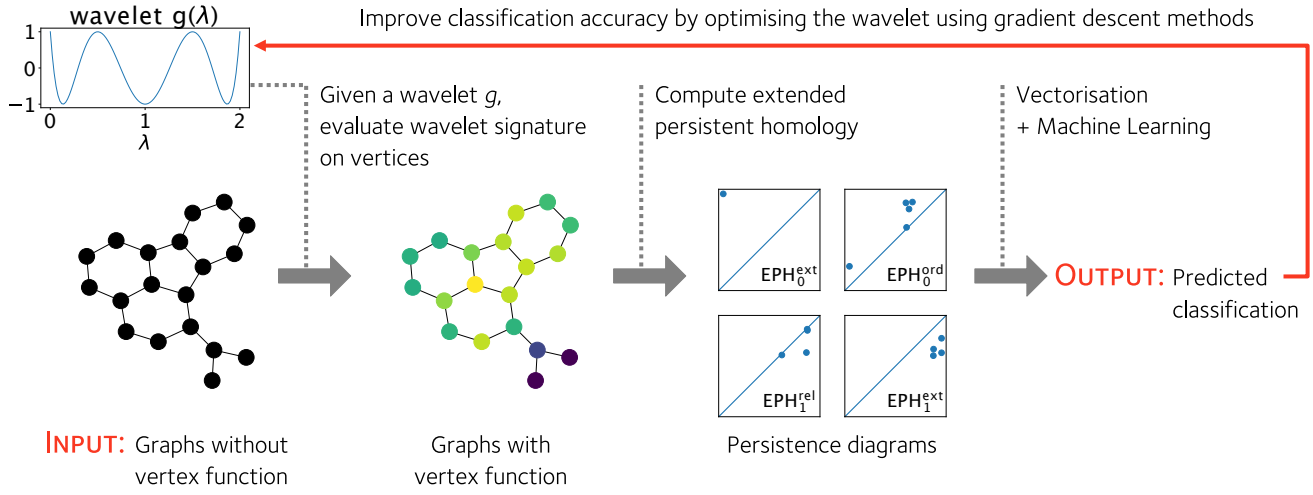


FIGURE 1. Given a wavelet $g : \mathbb{R} \rightarrow \mathbb{R}$, we can equip any graph with a non-trivial vertex function. This allows us to compute the extended persistence diagrams of a graph and use the diagrams as features of the graph to predict a graph’s classification in some real world setting. The wavelet g can be optimised to improve the classification accuracy of a graph classification pipeline based on the extended persistence diagrams of a graph’s vertex function.

1.2. Outline and Contributions. We address the issue of vertex function parametrisation and optimisation using *wavelet signatures*. Wavelet signatures are vertex functions derived from the eigenvalues and eigenvectors of the graph Laplacian and encode multiscale geometric information about the graph [LH13]. The wavelet signature of a graph is dependent on a choice of wavelet $g : \mathbb{R} \rightarrow \mathbb{R}$, a function on the eigenvalues of the graph’s Laplacian matrix. We can thus obtain a parametrisation of vertex functions for any graph $F : \mathcal{M} \rightarrow \mathbb{R}^V$ by parametrising g . Consequently, the extended persistence diagrams of a graph can be varied over the parameter space \mathcal{M} . If we have a function $\text{Out} : \mathbf{Bar}^4 \rightarrow \mathbb{R}$ on persistence diagrams that we wish to minimise, we can optimise over \mathcal{M} to minimise the loss function

$$\mathcal{L} : \mathcal{M} \xrightarrow{F} \mathbb{R}^V \xrightarrow{\text{EPH}} \mathbf{Bar}^4 \xrightarrow{\text{Out}} \mathbb{R}. \quad (1)$$

If \mathcal{L} is generically differentiable, we can optimise the wavelet signature parameters $\theta \in \mathcal{M}$ using gradient descent methods. We illustrate an application of this framework to a graph classification problem in Figure 1, where the loss function \mathcal{L} is the classification error of a graph classification prediction model based on the graph’s extended persistence diagrams.

In Section 2, we describe the assignment of vertex functions $F : \mathcal{M} \rightarrow \mathbb{R}^V$ by reviewing the definition of wavelet signatures. While spectral wavelets have been used in graph neural network architectures that predict vertex features [Xu+19] and compress vertex functions [RG19], they have not been considered in a persistence homology framework for graph classification. We describe several ways to parametrise wavelets. We also show in Proposition 2.2 that wavelet signatures are independent of the choice of

eigenbasis of the graph Laplacian from which it is derived, ensuring that it is well-defined. We prove this result in Appendix B.

In Section 3, we describe the theoretical basis for optimising the *extended* persistence homology of a vertex function $\mathcal{L} : \mathbb{R}^V \rightarrow \mathbf{Bar}^4$ and elucidate what it means for \mathcal{L} to be differentiable. In Proposition 3.3, we generalise the differentiability formalism of ordinary persistence [LOT19] to extended persistence. We prove this result in Appendix A

In Section 4, we show experimental results for optimising persistence for different choices of loss functions Out on persistence. We observe that our graph classification framework is successful in optimising the total persistence of graphs and graph classification accuracies for simple vectorisation methods. We also provide empirical evidence that some vectorisation methods may not mesh well with a vertex function optimisation framework based on gradient descent.

2. Filter Function Parametrization

We describe our recipe for assigning vertex functions to any simplicial graph $G = (V, E)$ based on a parametrised spectral wavelet, the first part F of the loss function

$$\mathcal{L} : \mathcal{M} \xrightarrow{F} \mathbb{R}^V \xrightarrow{\text{EPH}} \mathbf{Bar}^4 \xrightarrow{\text{Out}} \mathbb{R} . \quad (\text{Equation (1) recalled})$$

Our recipe is based on a graph's wavelet signature, a vertex function derived from the graph's Laplacian. The wavelet signature also depends on a so-called 'wavelet function' in $g : \mathbb{R} \rightarrow \mathbb{R}$, which is independent of the graph. By modulating the wavelet, we can jointly vary the wavelet signature across many graphs. Our method of using wavelet signatures to assign and parametrise vertex functions for computing extended persistence is a generalisation of the approach in Carrière et al. [Car+20b], where a fixed rather than variable wavelet called the heat kernel was employed. We parametrise the wavelet with finitely few parameters such that the wavelet signature can be manipulated in a computationally tractable way. In the following section, we define the wavelet signature and describe a linear approach to wavelet parametrisation.

2.1. Wavelet Signatures. The wavelet signature is a vertex function initially derived from wavelet transforms of vertex functions on graphs [HVG11], a generalisation of wavelet transforms for square integrable functions on Euclidean space [Gra95; Chu16] for signal analysis [Aka+01]. Wavelet signatures for graphs have been applied to encode geometric information about meshes of 3D shapes [Aka+01; LH13]. Special cases of wavelets signatures, such as the heat kernel signature [SOG09] and wave kernel signature [ASC11], have also been applied to describe graphs and 3D shapes [BK10; HRG14].

The wavelet signature of a graph is constructed from the graph's Laplacian operator. A graph's normalised Laplacian $L \in \mathbb{R}^{V \times V}$ is a symmetric positive semi-definite matrix, whose entries are given by

$$L_{uv} = \begin{cases} 1 & u = v \\ -\frac{1}{\sqrt{k_u k_v}} & (u, v) \in E \\ 0 & \text{otherwise} \end{cases} \quad (2)$$

where k_u is the degree of vertex u . The Laplacian's eigenvalues λ and eigenvectors ϕ are known to encode various topological and geometric information about the graph [CG97; BLS07]; for example, the number of zero eigenvalues corresponds to the number of connected components of the graph. The spectrum of the normalised Laplacian have real eigenvalues in $[0, 2]$ [CG97]. As such, any function $g : \mathbb{R} \rightarrow \mathbb{R}$ evaluated on the eigenvalues need only be defined on $[0, 2]$. Moreover, functions on a compact domain are easily parametrised using convenient bases.

Definition 2.1. [Wavelet Signature [LH13]] Let $L \in \mathbb{R}^{V \times V}$ be the normalised Laplacian of a simplicial graph $G = (V, E)$. Let $\phi_1, \dots, \phi_{|V|}$ be an orthonormal eigenbasis for L and $\lambda_1, \dots, \lambda_{|V|}$ be their corresponding eigenvalues. The wavelet signature $W : \mathbb{R}^{[0,2]} \rightarrow \mathbb{R}^V$ maps a function $g : [0, 2] \rightarrow \mathbb{R}$, which we refer to as a *wavelet*, to a vertex function $W(g) \in \mathbb{R}^V$ linearly, where the value of $W(g)$ on vertex v is given by

$$W(g)_v = \sum_{i=1}^{|V|} g(\lambda_i) (\phi_i)_v^2, \quad (3)$$

and $(\phi_i)_v$ denotes the component of eigenvector ϕ_i corresponding to vertex v .

If the eigenvalues of L have geometric multiplicity one (i.e. their eigenspaces are one dimensional), then the orthonormal eigenvectors are uniquely defined up to a choice of sign. It is then apparent from Equation (3) that the wavelet signature is independent of the choice of sign. However, if some eigenvalues have geometric multiplicity greater than one, then the orthonormal eigenvectors of L are uniquely defined up to orthonormal transformations in the individual eigenspaces. However, the wavelet signature is well-defined even when the multiplicities of eigenvalues are greater than one. This is the content of the next Proposition, whose proof is deferred to Appendix B.

Proposition 2.2. *The wavelet signature of a graph is independent of the choice of orthonormal eigenbasis for the Laplacian.*

Remark 2.3. In addition to the traditional view of wavelets from a spectral signal processing perspective [HVG11], we can also relate the wavelet signature of a vertex v to the degrees of vertices in some neighbourhood of v prescribed by g . Consider a wavelet $g : [0, 2] \rightarrow \mathbb{R}$. On a finite graph G , the normalised Laplacian L has at most $|V|$ many distinct eigenvalues. As such, there exists a polynomial $\hat{g}(x) = \sum_{n=0}^p a_n x^n$ of finite order that interpolates g at the eigenvalues $g(\lambda_i) = \hat{g}(\lambda_i)$. Therefore, $W(g) = W(\hat{g})$. Moreover, the vertex values assigned by $W(\hat{g})$ are the diagonal entries of the matrix polynomial $\hat{g}(L)$:

$$\hat{g}(L)_{vv} = \sum_{n=0}^p a_n (L^n)_{vv} = \sum_{i=1}^{|V|} \hat{g}(\lambda_i) (\phi_i)_v^2 = \sum_{i=1}^{|V|} g(\lambda_i) (\phi_i)_v^2 = W(g)_{vv}. \quad (4)$$

Furthermore, we can also write the matrix polynomial $\hat{g}(L)$ as a matrix polynomial in $A = I - L$, the *normalised adjacency matrix*. From the definition of L , we can compute the diagonal entry of a monomial A^r corresponding to vertex v as an inverse degree weighted count of paths¹ $[v_0, v_1, \dots, v_r]$ on the graph which begin and end on vertex $v = v_0 = v_r$ [New18]:

$$(A^r)_{vv} = \frac{1}{k_v} \sum_{[v, v_1, \dots, v_{r-1}, v]} \left(\prod_{l=1}^{r-1} \frac{1}{k_{v_l}} \right). \quad (5)$$

By expressing the wavelet signature as a matrix polynomial in A , we see that g controls how information at different length scales of the graph contribute to the wavelet signature. For instance, if g were an order p polynomial, then $W(g)_v$ only takes the degrees of vertices that are $\lfloor p/2 \rfloor$ away from v into account. As a corollary, since $W(g)$ can be specified by replacing g with a polynomial \hat{g} of order at most $|V| - 1$, the wavelet signature at a vertex is only dependent on the subgraph of G that is within $\lfloor |V| - 1 \rfloor / 2$ steps away from v .

2.2. Choosing a Space of Wavelets. We see from Remark 2.3 that the choice of wavelet g determines how the topology and geometry of the graph is reflected in the vertex function. Though the space of wavelets is potentially infinite dimensional, here we only consider wavelets $g_\theta(x)$ that are parametrised by a parameters θ in a finite dimensional manifold, so that we can easily optimise them using computational methods. In particular, we focus on wavelets written as a linear combination of m basis functions $h_1, \dots, h_m : [0, 2] \rightarrow \mathbb{R}$

$$g_\theta(x) := \sum_{j=1}^m \theta_j h_j(x) \quad (6)$$

This parametrisation of wavelets in turn defines a parametrisation of vertex functions $F : \mathbb{R}^m \rightarrow \mathbb{R}^V$ for our optimisation pipeline in eq. (1)

$$F : \quad \theta \in \mathbb{R}^m \quad \longmapsto \quad F(\theta) := W(g_\theta) \quad \in \mathbb{R}^V. \quad (7)$$

Since $W(g)$ is a linear function of the wavelet g , F is a linear transformation:

$$F(\theta) = W \left(\sum_{j=1}^m \theta_j h_j(x) \right) = \sum_{j=1}^m \theta_j W(h_j). \quad (8)$$

We can write F as a $|V| \times m$ matrix acting on a vector $[\theta_1, \dots, \theta_m]^\top \in \mathbb{R}^m$, whose columns are the vertex functions $W(h_j)$. We now proceed to describe several convenient choices of basis functions h_j .

2.2.1. Chebyshev Polynomials. Any Lipschitz continuous function on an interval can be well approximated by truncating its Chebyshev series at some finite order [TB97]. The Chebyshev polynomials $T_n : [-1, 1] \rightarrow \mathbb{R}$

$$T_n(x) = \cos(n \arccos(x)) \quad n \in \mathbb{N}_{\geq 0}. \quad (9)$$

form an orthonormal set of functions. We can thus consider $h_j(\lambda) = T_j(\lambda - 1)$, $j = 0, 1, \dots, m$ as a basis for wavelets. We exclude $T_1(x) = x$ in the linear combination as $W(T_1(1 - x)) = 0$ for graphs without

¹Here a path refers to a sequences of vertices that are connected to the next vertex in the sequence by an edge.

self loops.

2.2.2. Radial Basis Functions. In the machine learning community, a *radial function* refers loosely to a continuous monotonically decreasing function $\rho : \mathbb{R}_{\geq 0} \rightarrow \mathbb{R}_{\geq 0}$. There are many possible choices for ρ , for example,

$$\rho(r) = \frac{1}{\sqrt{\left(\frac{r}{\epsilon}\right)^2 + 1}} \quad (10)$$

for some $\epsilon \neq 0$. We can parametrise the wavelet by choosing $h_j(x) = \rho(\|x - x_j\|)$, where $x_j \in \mathbb{R}$ is a collection of ‘centroids’ which offset the radial basis function along \mathbb{R} . In general, the centroids are parameters that could be optimised, but we fix them in this study. This parametrisation can be considered as a *radial basis function neural network*. RBNNs are well-studied in function approximation and subsequently machine learning; we refer readers to [CCG91; PS91] for further details.

2.3. Finding a Suitable Parametrisation of Wavelet Space. If F is *poorly conditioned*, i.e. the singular values of F span many orders of magnitude, then the vertex function may be unstable with respect to small changes in the wavelet coefficients θ . This may lead to instabilities in the gradient descent optimisation of \mathcal{L} . We illustrate this point by considering the compact singular value decomposition of F

$$F = \sum_{k=1}^r \sigma_k \mathbf{u}_k \mathbf{v}_k^\top = \begin{bmatrix} & & & \\ \mathbf{u}_1 & \cdots & \mathbf{u}_r & \\ & & & \end{bmatrix} \begin{bmatrix} \sigma_1 & & \\ & \ddots & \\ & & \sigma_r \end{bmatrix} \begin{bmatrix} & & & \\ \mathbf{v}_1 & \cdots & \mathbf{v}_r & \\ & & & \end{bmatrix}^\top \quad (11)$$

where $r \leq \min\{m, |V|\}$ is the rank of the matrix, $\sigma_k > 0$ are the non-zero singular values of the matrix, and $\mathbf{u}_k \in \mathbb{R}^{|V|}$ and $\mathbf{v}_k \in \mathbb{R}^m$ are orthonormal sets of vectors respectively. In a gradient descent step, the wavelet coefficients are updated to $\theta \mapsto \theta - s\delta\theta$, where

$$\delta\theta = \nabla_\theta \mathcal{L} = \nabla_\theta f^\top \nabla_f \mathcal{L} = F^\top \nabla_f \mathcal{L} = \sum_{k=1}^r \sigma_k \langle \nabla_f \mathcal{L}, \mathbf{u}_k \rangle \mathbf{v}_k. \quad (12)$$

Correspondingly, the vertex function s is updated $f \mapsto f - s\delta f$ linearly with $\delta\theta$

$$\delta f = F \delta\theta = \sum_{k=1}^r \sigma_k^2 \langle \nabla_f \mathcal{L}, \mathbf{u}_k \rangle \mathbf{u}_k. \quad (13)$$

If the \mathcal{L} has large second derivatives – for example, due to nonlinearities in Out – the projections $\langle \mathbf{u}_k, \nabla_f \mathcal{L} \rangle$ in eqs. (12) and (13) may change dramatically from one gradient descent update to another. If the smallest singular value is much smaller than the largest, then updates to the wavelet signature can be especially unstable throughout the optimisation process.

We resolve this issue by finding a new orthonormal basis – for instance \mathbf{u}_k – for the space of vertex functions spanned by $W(h_1), \dots, W(h_m)$. We can derive a new parametrisation $F' : \mathbb{R}^r \rightarrow \mathbb{R}^V$ by expressing

a vertex function as a linear combination in the new basis

$$f = \theta'_1 \mathbf{u}_1 + \cdots + \theta'_r \mathbf{u}_r = \begin{bmatrix} | & & | \\ \mathbf{u}_1 & \cdots & \mathbf{u}_r \\ | & & | \end{bmatrix} \theta' =: \mathbf{F}' \theta'. \quad (14)$$

As \mathbf{u}_k are orthonormal, the non-zero singular values of \mathbf{F}' are all one. Thus, the gradient descent updates are stabilised. In particular, the update to f is simply the projection of $\nabla_f \mathcal{L}$ onto our space of wavelet signatures:

$$\delta f = \sum_{k=1}^r \langle \mathbf{u}_k, \nabla_f \mathcal{L} \rangle \mathbf{u}_k. \quad (15)$$

Remark 2.4 (Stabilising Optimisation over Multiple Graphs). In the case where we are optimising a wavelet jointly over graphs G_1, \dots, G_N , we would like a parametrisation that stabilises updates on all graphs. We can view the maps F_1, \dots, F_N that map wavelet basis coefficients to vertex functions of graphs G_1, \dots, G_N respectively as a parametrisation for the disjoint union $\bigsqcup_i G_i$:

$$f = \begin{bmatrix} f_1 \\ \vdots \\ f_N \end{bmatrix} = \begin{bmatrix} \mathbf{F}_1 \\ \vdots \\ \mathbf{F}_N \end{bmatrix} \theta =: \mathbf{F} \theta. \quad (16)$$

We can then choose an orthonormal basis for the space spanned by column vectors of \mathbf{F} to generate a new parametrisation \mathbf{F}' across all graphs.

Remark 2.5 (Generalising Parameters to New Graphs). Suppose we have a vertex function $f = \sum_{k=1}^r \theta'_k \mathbf{u}_k$ defined on a fixed set of graphs. Using the linearity of W and the fact that \mathbf{u}_k are obtained from the singular value decomposition of \mathbf{F} , we can rewrite f as

$$f = \sum_{k=1}^r \theta'_k \mathbf{u}_k = \sum_{k=1}^r \theta'_k \frac{1}{\sigma_k} \sum_{j=1}^m (\mathbf{v}_k)_j W(h_j) = W \left(\underbrace{\sum_{j=1}^m \sum_{k=1}^r (\mathbf{v}_k)_j \frac{\theta'_k}{\sigma_k} h_j}_{\tilde{g}} \right). \quad (17)$$

We can then use the wavelet \tilde{g} the parentheses to compute wavelet signatures on new graphs.

3. Extended Persistent Homology

The homology of a given graph is a computable vector space whose dimension counts the number of connected components or cycles in the graph. Finer information can be retained by filtering the graph and analysing the evolution of the homology throughout the filtration. This evolution is described by a set of *extended persistence diagrams* (a.k.a. *extended barcodes*), a multiset of points $\langle b, d \rangle$ that record the birth b and death of homological features in the filtration. In this section, we begin by summarising these constructions. We refer the reader to Zomorodian and Carlsson [ZC05], Edelsbrunner and Harer, [EH08] and Cohen-Steiner, Edelsbrunner, and Harer [CEH07] for full treatments of the theory of Persistence.

Compared to *ordinary persistence*, extended persistence is a more informative and convenient feature map for graphs. Extended persistence encodes strictly more information than ordinary persistence. For instance, the cycles of a graph are represented as points with $d = \infty$ in ordinary persistence. Thus, only the birth coordinate b of such points contain useful information about the cycles. In contrast, the corresponding points in extended persistence are each endowed with a finite death time d , thus associating extra information to the cycles. The points at infinity in ordinary persistence also introduce obstacles to vectorisation procedures, as often arbitrary finite cutoffs are needed to ‘tame’ the persistence diagrams before vectorisation.

3.1. Extended Persistent Homology. Let $G = (V, E)$ be a finite graph without double edges and self-loops. For the purposes of this paper, the associated *extended persistent homology* is a map

$$\text{EPH} : \mathbb{R}^V \rightarrow \mathbf{Bar}^4$$

from functions $f \in \mathbb{R}^V$ on its vertices to the space of four *persistence diagrams* or *barcodes*, which we define below. The map arises from a *filtration* of the graph, a sequential attachment of vertices and edges in ascending or descending order of f . We extend f on each edge $e = (v, v')$ by the maximal value of f over the vertices v and v' , and we then let $G_t \subset G$ be the sub graph induced by vertices taking value less than t . Then we have the following sequence of inclusions:

$$\emptyset \longrightarrow \dots \longrightarrow G_s \xrightarrow{s \leq t} G_t \longrightarrow \dots \longrightarrow G. \quad (18)$$

Similarly, the sub graphs $G^t \subset G$ induced by vertices taking value greater than t assemble into a sequence of inclusions:

$$G \leftarrow \dots \leftarrow G^s \xleftarrow{s \leq t} G^t \leftarrow \dots \leftarrow \emptyset. \quad (19)$$

The changes in the topology of the graph along the filtration in ascending and descending order of f can be detected by its *extended persistence module*, indexed over the poset $\mathbb{R} \cup \{\infty\} \cup \mathbb{R}^{\text{op}}$:

$$\begin{aligned}
0 = H_p(\emptyset) &\longrightarrow \cdots \longrightarrow H_p(G_s) \xrightarrow{s \leq t} H_p(G_t) \longrightarrow \cdots \longrightarrow H_p(G) \\
\mathbb{V}_p(f) : & & & \downarrow \cong & , & (20) \\
0 = H_p(G, G) &\leftarrow \cdots \leftarrow H_p(G, G^s) \xleftarrow{s \leq t} H_p(G, G^t) \leftarrow \cdots \leftarrow H_p(G, \emptyset)
\end{aligned}$$

where H_p is the singular (relative) homology functor in degree $p \in 0, 1$ with coefficients in a fixed field, chosen to be $\mathbb{Z}/2\mathbb{Z}$ in practice. In general terms, the modules $V_0(f)$ and $V_1(f)$ together capture the evolution of the connected components and loops in the sub graphs of G induced by the function f .

Each module $V_p(f)$ is completely characterised by a finite multi-set $EPH_p(f)$ of pairs of real numbers $\langle b, d \rangle$ called *intervals* representing the birth and death of homological features. Following Cohen-Steiner, Edelsbrunner, and Harer [CEH09], the intervals in $EPH_p(f)$ are further partitioned according to the type of homological feature they represent:

$$\text{EPH}_p(f) = \underbrace{\{\langle b, d \rangle \mid b < d < \infty\}}_{=\text{EPH}_p^{\text{ord}}(f)} \sqcup \underbrace{\{\langle b, d \rangle \mid b < \infty < d\}}_{=\text{EPH}_p^{\text{ext}}(f)} \sqcup \underbrace{\{\langle b, d \rangle \mid \infty < b < d\}}_{=\text{EPH}_p^{\text{rel}}(f)}. \quad (21)$$

Each of the three finite multiset $\text{EPH}_p^k(f)$, for $k \in \{\text{ord}, \text{ext}, \text{rel}\}$, is an element in the space \mathbf{Bar} of so-called *barcodes* or *persistence diagrams*. However, $\text{EPH}_0^{\text{rel}}(f)$ and $\text{EPH}_1^{\text{ord}}(f)$ being trivial for graphs, we refer to the collection of four remaining persistence diagrams

$$\text{EPH}(f) = [\text{EPH}_0^{\text{ord}}(f), \text{EPH}_0^{\text{ext}}(f), \text{EPH}_1^{\text{ext}}(f), \text{EPH}_1^{\text{rel}}(f)] \in \mathbf{Bar}^4 \quad (22)$$

as the *extended barcode* or *extended persistence diagram* of f . We have thus defined the *extended persistence map*

$$\text{EPH} : \mathbb{R}^V \rightarrow \mathbf{Bar}^4.$$

Remark 3.1. If we only apply homology to the filtration of Eq. (18), we get an *ordinary persistence module* indexed over the real line, which is essentially the first row in Eq. (20). This module is characterised by a unique barcode $\text{PH}_p(f) \in \mathbf{Bar}$. We refer to the map

$$\text{PH} : f \in \mathbb{R}^V \longmapsto [\text{PH}_0(f), \text{PH}_1(f)] \in \mathbf{Bar}^2 \quad (23)$$

as the *ordinary persistence map*.

3.2. Differentiability of Extended Persistence. The extended persistence map can be shown to be locally Lipschitz by the Stability theorem [CEH09]. The Rademacher theorem states that any real-valued function that is locally Lipschitz is differentiable on a full measure set. Thus so is our loss $\text{Out} \circ \text{EPH} \circ \text{F}$ as long as the maps Out and F are smooth or locally Lipschitz, which enables the use of stochastic gradient descent as a paradigm of optimisation. Nonetheless, the above theorem does not prevent dense sets of non differentiability in general.

In this section, we show that the set where EPH is not differentiable is not pathological. Namely, we show that EPH is *generically* differentiable, i.e. differentiable on an open dense subset. This property guarantees that local gradients yield reliable descent directions in a neighbourhood of the current iterate. We recall from Leygonie, Oudot, and Tillmann [LOT19] the definition of differentiability for maps to barcodes.

We call a map $\text{F} : \mathcal{M} \rightarrow \mathbb{R}^V$ a *parametrisation*, as it corresponds to a selection of filter functions over G parametrised by the manifold \mathcal{M} . Then $B := \text{EPH} \circ \text{F}$ is the barcode valued map whose differentiability properties are of interest in applications.

Definition 3.2. A map $B : \mathcal{M} \rightarrow \mathbf{Bar}$ on a smooth manifold \mathcal{M} is said to be differentiable at $\theta \in \mathcal{M}$ if for some neighbourhood U of θ , there exists a finite collection of differentiable maps ² $b_i, d_i : U \rightarrow \mathbb{R} \cup \{\infty\}$,

²By convention, a differentiable map that takes the value ∞ is constant.

called a *local coordinate system* for B at θ , such that

$$\forall \theta' \in U, B(\theta') = \{\langle b_i(\theta'), d_i(\theta') \rangle \mid b_i(\theta') \neq d_i(\theta')\}.$$

For $N \in \mathbb{N}$, we say that a map $B : \mathcal{M} \rightarrow \mathbf{Bar}^N$ is differentiable at θ if all its components are so.

In Leygonie, Oudot, and Tillmann [LOT19], it is proven that the composition $\text{PH} \circ F$ is generically differentiable as long as F is so. It is possible to show that $\text{EPH} \circ F$ is generically differentiable along the same lines, but we rather provide an alternative argument in the appendix. Namely, we rely on the fact that the extended persistence of G can be decoded from the ordinary persistence of the cone complex $\text{Cone}(G)$, a connection first noted in Cohen-Steiner, Edelsbrunner, and Harer [CEH09] for computational purposes.

Proposition 3.3. *Let $F : \mathcal{M} \rightarrow \mathbb{R}^V$ be a generically differentiable parametrisation. Then the composition $\text{EPH} \circ F$ is generically differentiable.*

For completeness, the proof provided in the appendix treats the general case of a finite simplicial complex K of arbitrary dimension.

4. Experiments

We perform experiments where we minimise different types of loss functions Out in our wavelet signature optimisation framework eq. (1). In supervised learning, we wish to *generalise* information on some *known data* G° to make claims about *new data* G^\bullet . If the minima of \mathcal{L}_{G° are close to those of \mathcal{L}_{G^\bullet} , then learning appropriate wavelets that minimise \mathcal{L}_{G° on known data is useful for supervised learning tasks on dataset of graphs. Heuristically, this would hold true if the ‘distribution’ of G^\bullet is similar to that of G° when they are embedded in \mathbf{Bar}^4 via the map $\text{EPH} \circ F : \mathcal{M} \rightarrow \mathbf{Bar}^4$.

We test this hypothesis by minimising different forms of \mathcal{L}_G on real world datasets of graphs - graphs that are grouped together in real world empirical contexts. The graphs in the datasets [RA15] we examine - MUTAG, COX2, DHFR, and NCI1 - represent structures of molecules of biomedical interest. We employ a 10 tenfold test-train split scheme on each dataset G to test the hypothesis: in each ‘fold’, we randomly designate a tenth of a dataset G as a ‘test set’ G^\bullet , and the remainder as the known ‘training set’ G° , on which we optimise θ using gradient descent methods. The learnt parameter θ is then validated by computing the corresponding test accuracy on G^\bullet . Each ten-fold is a different random partition of the dataset into ten portions which take turn to be the test set.

4.1. Maximising Persistence. As a simple example, suppose we would like to learn a wavelet γ_θ that maximises

$$\mathcal{L}(\theta) = \sum_{D \in \text{EPH}(\gamma_\theta)} \text{TP}_2(D). \quad (24)$$

where $\text{TP}_2 : \mathbf{Bar}^4 \rightarrow \mathbb{R}$ is the sum of persistence squared of bars in all four persistence diagrams $D \in \mathbf{Bar}^4$

$$\text{TP}_2(D) = \sum_{i \in D} (d_i - b_i)^2.$$

We parametrise our wavelet using an order 6 Chebyshev polynomial, where $\theta \in \mathbb{S}^5$, constraining the Chebyshev coefficients $\sum_i \theta_i^2 = 1$. This avoids the algorithm learning a trivial solution of rescaling the vertex function by a constant.

We tested this on two datasets of small molecules, MUTAG and COX2. As shown in fig. 2, we compute the objective function evaluated on the training dataset G° and test dataset G^\bullet respectively; the curves trace the medians of the objective functions over 10 ten-folds as a function of the number of gradient steps taken by the stochastic gradient descent algorithm.

For both datasets, we observe that the Chebyshev coefficients successfully evolved to increase \mathcal{L} on the training dataset G° . Successive gradient steps also increase \mathcal{L} on the test data G^\bullet , with good agreement between the values of the objective functions on the test and train data. This is positive evidence towards the hypothesis that wavelets can be learnt to optimise functions on extended persistence diagrams. Furthermore, a wavelet learnt on known data G° can generalise to optimising \mathcal{L} on new data G^\bullet .

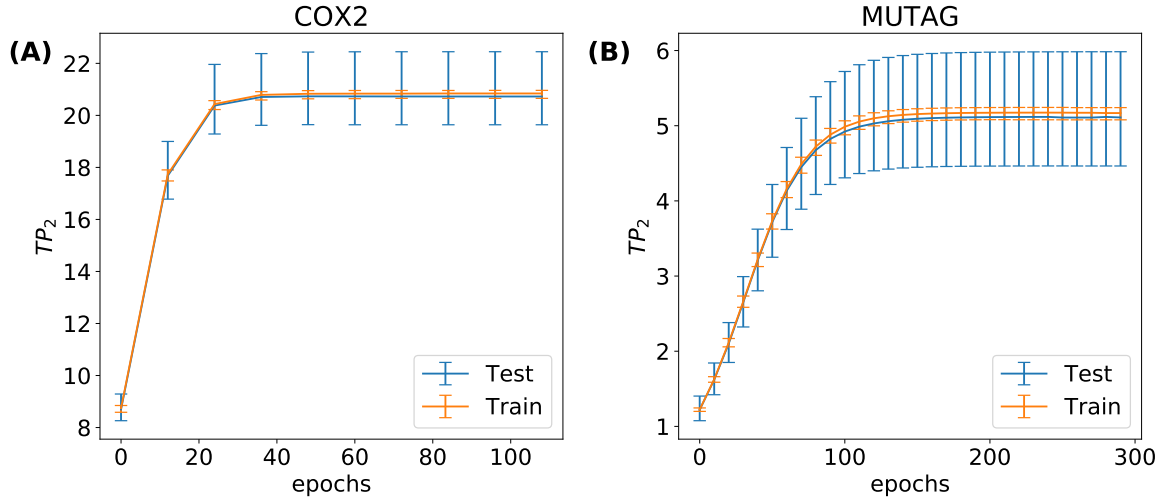


FIGURE 2. Average total 2-persistence of the extended persistence diagrams of graphs in (A) COX2 and (B) MUTAG respectively, as a function of wavelet parameters along the gradient descent trajectory of the stochastic gradient descent algorithm on training and test datasets G° and G^\bullet respectively. The curve denotes the median of the objective functions over 10 ten-folds, while the errorbars denote the 5% to 95% quantiles.

4.2. Binary graph classification. In a more realistic application, we investigate whether optimising the extended persistence of wavelet signatures can be usefully applied to *graph classification* problems,

where persistence diagrams are used as features to predict discrete, ‘real life’ attributes of networks. In this setting, we aim to learn $\theta \in \mathcal{M}$ that minimise the *classification error* of graphs over a training data set of $G \in \mathbf{G}^\circ$.

Compared to TP_2 , the classification error that we wish to minimise

$$\mathcal{L} : \mathcal{M} \xrightarrow{F} \mathbb{R}^V \xrightarrow{\text{EPH}} \mathbf{Bar}^4 \xrightarrow{\text{Out}} \mathbb{R}. \quad (\text{eq. (1)})$$

is more complex in the construction of the map *Out*. The map *Out* is a composition of two maps: a classifier that predicts the class of a graph, composed with a map to \mathbb{R} that quantifies the error in the prediction. In our experiments, we minimise the *binary cross entropy* between the predicted labels by the model and the true labels in the data. We use a linear combination of n radial basis functions $\rho(|x - x_j|)$ to parametrise the wavelets, where ρ is given by eq. (10) and the n centroids x_j are located at $x_j = 2j/(n-3)$, $j = -1, 0, \dots, n-2$. The width parameter ϵ of the radial basis function eq. (10) is chosen to be $\epsilon = 2/(n-3)$. The parametrisation of vertex functions for different experiments are specified in table 1, table 2, and table 3 alongside the architecture performances. In some experiments, the wavelet parameters are simply the coefficients θ of the basis functions, while in others the parameters are the coefficients θ' for the vertex functions u_k obtained from the singular value decomposition of F . We refer to the latter parameters θ' as ‘latent’ parameters. In some experiments employing latent parameters, we restrict coefficients θ' to those corresponding to vertex functions u_k that have the top k singular values.

For each experiment where the wavelet is optimised, we also perform a *control experiment* where we fix the wavelet and only optimise the parameters of the neural networks, whose architecture stays constant. The control experiment functions as a baseline against which we assess the efficacy of wavelet optimisation. We choose the wavelet to be $g(\lambda) = \exp(-10\lambda)$, the heat kernel signature [BK10] with scale parameter $t = 10$ used in PersLay for those datasets [Car+20b].

We apply our framework to classifying graphs in the datasets MUTAG, DHFR, COX2 and NCI1. These datasets consist of the graphs representing the molecular structure of small biochemical molecules. We measure the classification accuracy using the same metrics as Carrière et al. [Car+20b], where we take a known dataset of labelled graphs and perform a 10 ten-fold test-train split. The accuracy of a classifier is averaged over all one hundred tests. We use the [GUDHI](#) library to compute persistence, and make use of the optimisation and machine learning library PyTorch for the construction of the graph classifications models.

We compare how the wavelet optimisation affects the accuracy of models of varying complexity of the vectorisation and classification architecture *Out*.

4.2.1. *Simple Vectorisation + Linear Classifier.* We use a simple vectorisation method modelled on the approach proposed in Adcock, Carlsson, and Carlsson [ACC13]. We map each diagram D to the vector

$$D \mapsto \left[\sum_{i \in D} p_i, \log \left(\sum_{i \in D} \exp(p_i) \right), \sum_{i \in D} b_i p_i, \sum_{i \in D} d_i p_i, \sum_{i \in D} b_i \log(1 + p_i) \sum_{i \in D} d_i \log(1 + p_i) \right]; \quad (25)$$

where $p_i = d_i - b_i$.

The first term is the sum of the persistence of the bars, the second term is a ‘smoothed maximum’ of the persistence of the points, and the remaining terms are weighted sums of births and deaths of a barcode, where the weights are positive increasing functions of persistence

We then apply an affine transformation to map the vectorised persistence diagrams of a graph to a real number, whose sign determines the predicted label of the class. The details of the experimental implementation are described in Appendix C.1.

We show the classification accuracies in table 1. We observe that the wavelet optimisation does yield an improvement to the classification accuracy compared to using a fixed the heat kernel signature. In particular, we observe that an optimised choice of wavelets produced a significant gain in classification accuracy on the DHFR dataset.

4.2.2. *Simple Vectorisation + Neural Network Classifier.* We use the same vectorisation method as Section 4.2.1, but we replaced the linear classifier with a neural network with one hidden layer. The details of the experimental implementation are described in Appendix C.2.

We show the classification accuracies in table 2. Given the greater expressiveness of the neural network compared to a linear classifier, we observe an increase in the classifier accuracy for our model and the control model where the wavelet is fixed. Comparing our optimised model to the control model, we observe that the optimised model continues to outperform the fixed the heat kernel signature on all datasets apart from MUTAG, where the performance of either models are statistically indistinguishable.

4.2.3. *Persistence Images and Convolutional Neural Networks.* We use persistence images as the vectorisation method and applied a convolutional neural network to map the vectorised diagrams to a classification, adopting an architecture proposed in Carrière et al. [Car+20b]. We computed and optimised the latent parameters rather than the radial basis function coefficients on all datasets, as we observed instabilities in using the radial basis function coefficients as the wavelet parameter space, unlike in the previous experiments. We attribute this to the greater complexity and nonlinearity in the loss function. As we had noted in Section 2.3, poorly conditioned basis function coefficients are especially liable to instabilities in gradient descent updates. In contrast, the well conditioned latent parameters suffered no instabilities in the gradient descent updates. The details of the experimental implementation are described in Appendix C.3.

We show the classification accuracies in table 3. Comparing our optimised model to the control model, we observe that the optimised model overfits on the smaller datasets MUTAG and COX2, but continues to yield improvements on the larger datasets DHFR and NCI1 .

5. Conclusion

We have presented a framework for equipping any graph G with a set of extended persistence diagrams $\text{EPH} \circ F : \mathcal{M} \rightarrow \mathbf{Bar}$ parametrised over a manifold \mathcal{M} , using linear parametrisations of the graph's inherent wavelet signatures. Given a function on persistence diagrams, $\text{Out} : \mathbf{Bar} \rightarrow \mathbb{R}$ that is differentiable, we can define gradients of $\mathcal{L} = \text{Out} \circ \text{EPH} \circ F$ with respect to $\theta \in \mathcal{M}$ as \mathcal{L} can be shown to be generically differentiable. Thus, we can apply gradient descent methods to optimise the extended persistence diagrams of a graph to minimise \mathcal{L} .

We have shown that a loss function defined on the persistence diagrams of multiple graphs belonging to a dataset can be minimised on a parameter space of wavelets using gradient descent methods. In particular, wavelet optimisation improves the accuracy of graph classification of linear classifiers across several benchmark datasets. We also observe that loss functions whose Out component involves nonlinear transformations, such as the combination of persistence images with convolutional neural networks, may lead to a loss landscape with irregular gradients and hamper applications to graph classification problems. To incorporate persistence optimisation into a machine learning framework, further consideration must be put into the selection of vectorisation methods that enable effective vertex functions optimisation via persistence.

Conflict of Interest Statement

The authors declare that the research was conducted in the absence of any commercial or financial relationships that could be construed as a potential conflict of interest.

Author Contributions

The overall framework was jointly conceived by both authors. KMY was responsible for developing wavelet signatures as a vertex function parametrisation framework, along with the experimental design and analysis. The proof of the differentiability of extended persistence is due to JL. Both authors participated in the writing of the article.

Funding

Ka Man Yim is funded by the EPSRC Centre For Doctoral Training in Industrially Focused Mathematical Modelling (EP/L015803/1) with industrial sponsorship from Elsevier. Jacob Leygonie is funded by

the EPSRC grant EP/R513295/1. Both authors are members of the Centre for Topological Data Analysis, which is supported by the EPSRC grant New Approaches to Data Science: Application Driven Topological Data Analysis EP/R018472/1.

Acknowledgments

The authors would like to thank Ulrike Tillmann and Heather Harrington for their close guidance and thoughtful advice on this project. In addition, the authors would like to thank Vidit Nanda, Peter Grindrod CBE, Steve Oudot, Mathieu Carrière, and Theo Lacombe for fruitful discussions on this subject.

Data Availability Statement

The code for the computational experiments in section 4 can be found in the GitHub repository https://github.com/kmyim/Persistence_Opt_Spectral_Wavelets. The datasets we use are publicly available at <http://networkrepository.com> [RA15].

Dataset	# RBF	Parametrisation	Test Accuracy	Control (HKS10)
MUTAG	10	RBF coefficients	86.9 \pm 1.8	85.9 \pm 1.0
COX2	12	RBF coefficients	78.7 \pm 0.9	77.9 \pm 0.3
DHFR	10	RBF coefficients	74.3 \pm 0.7	67.9 \pm 0.6
NCI1	12	RBF coefficients	66.9 \pm 0.3	65.6 \pm 0.2

TABLE 1. Binary classification accuracy on a datasets of graphs of small molecules, where a linear classifier is applied to the vectorised persistence diagrams. Accuracies quoted are the mean over 10 ten-fold experiments, and the error quoted correspond to standard deviations across the 10 *mean* accuracies of each ten-fold. The classifier model is described in appendix C and section 4.2.1.

Dataset	# RBF	Parametrisation	Test Accuracy	Control (HKS10)
MUTAG	10	RBF coefficients	86.8 \pm 1.2	86.2 \pm 1.3
COX2	12	RBF coefficients	79.6 \pm 1.0	78.3 \pm 0.4
DHFR	12	Latent parameters (3)	78.7 \pm 0.7	78.0 \pm 0.9
NCI1	12	Latent parameters (12)	71.1 \pm 0.3	70.2 \pm 0.3

TABLE 2. Binary classification accuracy on a datasets of graphs of small molecules, where a neural network with one hidden layer is applied to the vectorised persistence diagrams. Accuracies quoted are the mean over 10 ten-fold experiments, and the error quoted correspond to standard deviations across the 10 *mean* accuracies of each ten-fold. The classifier model is described in appendix C and section 4.2.2.

Dataset	# RBF	Parametrisation	Test Accuracy	Control (HKS10)
MUTAG	12	Latent parameters (3)	84.8 \pm 1.3	86.5 \pm 1.2
COX2	12	Latent parameters (3)	79.1 \pm 0.6	79.8 \pm 0.4
DHFR	12	Latent parameters (3)	79.1 \pm 1.1	78.2 \pm 1.0
NCI1	12	Latent parameters (12)	72.8 \pm 0.4	71.9 \pm 0.4

TABLE 3. Binary classification accuracy on a datasets of graphs of small molecules, where a convolutional neural network architecture is applied to the persistence images of the extended persistence diagrams. Accuracies quoted are the mean over 10 ten-fold experiments, and the error quoted correspond to standard deviations across the 10 *mean* accuracies of each ten-fold. The classifier model is described in appendix C.3 and section 4.2.3.

		Accuracy reported at epoch				Batch size			
		MUTAG	COX2	DHFR	NCI1	MUTAG	COX2	DHFR	NCI1
Table 1	RBF	200	200	200	200	17	36	31	137
	Control	400	200	1000	500	17	36	31	137
Table 2	RBF	200	200	175	125	17	36	11	20
	Control	400	200	1000	150	17	36	11	20
Table 3	RBF	150	50	100	125	10	9	11	20
	Control	200	75	150	200	10	9	11	20

TABLE 4. Experimental settings for performances reported in Section 4. Accuracy reported are best out of epochs of multiples of 25.

	Early stopping epoch for γ				γ parameter initialisation			
	MUTAG	COX2	DHFR	NCI1	MUTAG	COX2	DHFR	NCI1
Table 1	–	–	–	–	$\theta \sim \mathcal{N}(0, 1/\sqrt{\#\theta})$			
Table 2	–	–	–	20	$\theta \sim \mathcal{N}(0, 1/\sqrt{\#\theta})$	$\theta'_k = \langle u_k, W(\exp(-10x)) \rangle$		
Table 3	50	50	50	20		$\theta'_k = \langle u_k, W(\exp(-10x)) \rangle$		

TABLE 5. Early stopping epochs for the optimisation of wavelet parameters in the graph classification experiments described in Section 4. In experiments where the basis functions coefficients θ are the parameters being optimised, the initial coefficients are randomly drawn from a normal distribution. In experiments where we use latent parameters θ' , the latent parameters are initialised using a least squares fit to the wavelet signature to the heat kernel signature with diffusion parameter $t = 10$.

References

- [CCG91] Sheng Chen, Colin FN Cowan, and Peter M Grant. "Orthogonal least squares learning algorithm for radial basis function networks". In: *IEEE Transactions on neural networks* 2.2 (1991), pp. 302–309.
- [PS91] Jooyoung Park and Irwin W Sandberg. "Universal approximation using radial-basis-function networks". In: *Neural computation* 3.2 (1991), pp. 246–257.
- [Gra95] Amara Graps. "An introduction to wavelets". In: *IEEE computational science and engineering* 2.2 (1995), pp. 50–61.
- [CG97] Fan RK Chung and Fan Chung Graham. *Spectral graph theory*. 92. American Mathematical Soc., 1997.
- [TB97] Lloyd N Trefethen and David Bau III. *Numerical linear algebra*. Vol. 50. Siam, 1997.
- [Aka+01] Ali N Akansu et al. *Multiresolution signal decomposition: transforms, subbands, and wavelets*. Academic press, 2001.
- [ZC05] Afra Zomorodian and Gunnar Carlsson. "Computing persistent homology". In: *Discrete & Computational Geometry* 33.2 (2005), pp. 249–274.
- [BLS07] Türker Biyikoglu, Josef Leydold, and Peter F Stadler. *Laplacian eigenvectors of graphs: Perron-Frobenius and Faber-Krahn type theorems*. Springer, 2007.
- [CEH07] David Cohen-Steiner, Herbert Edelsbrunner, and John Harer. "Stability of persistence diagrams". In: *Discrete & Computational Geometry* 37.1 (2007), pp. 103–120.
- [EH08] Herbert Edelsbrunner and John Harer. "Persistent homology-a survey". In: *Contemporary mathematics* 453 (2008), pp. 257–282.
- [CEH09] David Cohen-Steiner, Herbert Edelsbrunner, and John Harer. "Extending persistence using Poincaré and Lefschetz duality". In: *Foundations of Computational Mathematics* 9.1 (2009), pp. 79–103.
- [She+09] Nino Shervashidze et al. "Efficient graphlet kernels for large graph comparison". In: *Artificial Intelligence and Statistics*. 2009, pp. 488–495.
- [SOG09] Jian Sun, Maks Ovsjanikov, and Leonidas Guibas. "A concise and provably informative multi-scale signature based on heat diffusion". In: *Computer graphics forum*. Vol. 28. 5. Wiley Online Library. 2009, pp. 1383–1392.
- [BK10] Michael M Bronstein and Iasonas Kokkinos. "Scale-invariant heat kernel signatures for non-rigid shape recognition". In: *2010 IEEE Computer Society Conference on Computer Vision and Pattern Recognition*. IEEE. 2010, pp. 1704–1711.
- [Vis+10] S Vichy N Vishwanathan et al. "Graph kernels". In: *The Journal of Machine Learning Research* 11 (2010), pp. 1201–1242.
- [ASC11] Mathieu Aubry, Ulrich Schlickewei, and Daniel Cremers. "The wave kernel signature: A quantum mechanical approach to shape analysis". In: *2011 IEEE international conference on computer vision workshops (ICCV workshops)*. IEEE. 2011, pp. 1626–1633.

- [HVG11] David K Hammond, Pierre Vandergheynst, and Rémi Gribonval. “Wavelets on graphs via spectral graph theory”. In: *Applied and Computational Harmonic Analysis* 30.2 (2011), pp. 129–150.
- [ACC13] Aaron Adcock, Erik Carlsson, and Gunnar Carlsson. “The ring of algebraic functions on persistence bar codes”. In: *arXiv preprint arXiv:1304.0530* (2013).
- [LH13] Chunyuan Li and A Ben Hamza. “A multiresolution descriptor for deformable 3D shape retrieval”. In: *The Visual Computer* 29.6-8 (2013), pp. 513–524.
- [HRG14] Nan Hu, Raif M Rustamov, and Leonidas Guibas. “Stable and informative spectral signatures for graph matching”. In: *Proceedings of the IEEE Conference on Computer Vision and Pattern Recognition*. 2014, pp. 2305–2312.
- [KB14] Diederik P Kingma and Jimmy Ba. “Adam: A method for stochastic optimization”. In: *arXiv preprint arXiv:1412.6980* (2014).
- [Sri+14] Nitish Srivastava et al. “Dropout: a simple way to prevent neural networks from overfitting”. In: *The journal of machine learning research* 15.1 (2014), pp. 1929–1958.
- [Tur+14] Katharine Turner et al. “Fréchet means for distributions of persistence diagrams”. In: *Discrete & Computational Geometry* 52.1 (2014), pp. 44–70.
- [RA15] Ryan A. Rossi and Nesreen K. Ahmed. “The Network Data Repository with Interactive Graph Analytics and Visualization”. In: *AAAI*. 2015. URL: <http://networkrepository.com>.
- [Chu16] Charles K Chui. *An introduction to wavelets*. Elsevier, 2016.
- [GHO16] Marcio Gameiro, Yasuaki Hiraoka, and Ippei Obayashi. “Continuation of point clouds via persistence diagrams”. In: *Physica D: Nonlinear Phenomena* 334 (2016), pp. 118–132.
- [New18] Mark Newman. *Networks*. Oxford university press, 2018.
- [OS18] Steve Oudot and Elchanan Solomon. “Inverse Problems in Topological Persistence: a Survey”. In: (2018).
- [PSO18] Adrien Poulard, Primoz Skraba, and Maks Ovsjanikov. “Topological function optimization for continuous shape matching”. In: *Computer Graphics Forum*. Vol. 37. 5. Wiley Online Library. 2018, pp. 13–25.
- [Che+19] Chao Chen et al. “A Topological Regularizer for Classifiers via Persistent Homology”. In: *The 22nd International Conference on Artificial Intelligence and Statistics*. 2019, pp. 2573–2582.
- [Clo+19] James R Clough et al. “Explicit topological priors for deep-learning based image segmentation using persistent homology”. In: *International Conference on Information Processing in Medical Imaging*. Springer. 2019, pp. 16–28.
- [Hof+19a] Christoph D Hofer et al. “Graph Filtration Learning”. In: *arXiv preprint arXiv:1905.10996* (2019).
- [Hof+19b] Christoph Hofer et al. “Connectivity-optimized representation learning via persistent homology”. In: *International Conference on Machine Learning*. PMLR. 2019, pp. 2751–2760.
- [Hu+19] Xiaoling Hu et al. “Topology-preserving deep image segmentation”. In: *Advances in Neural Information Processing Systems*. 2019, pp. 5658–5669.
- [LOT19] Jacob Leygonie, Steve Oudot, and Ulrike Tillmann. “A Framework for Differential Calculus on Persistence Barcodes”. In: *arXiv preprint arXiv:1910.00960* (2019).

[Moo+19] Michael Moor et al. “Topological autoencoders”. In: *arXiv preprint arXiv:1906.00722* (2019).

[RG19] Raif M Rustamov and Leonidas J Guibas. “Wavelets on graphs via deep learning”. In: *Vertex-Frequency Analysis of Graph Signals*. Springer, 2019, pp. 207–222.

[Xu+19] Bingbing Xu et al. “Graph wavelet neural network”. In: *arXiv preprint arXiv:1904.07785* (2019).

[ZW19] Qi Zhao and Yusu Wang. “Learning metrics for persistence-based summaries and applications for graph classification”. In: *Advances in Neural Information Processing Systems*. 2019, pp. 9859–9870.

[Brü+20] Rickard Brüel-Gabrielsson et al. “Topology-Aware Surface Reconstruction for Point Clouds”. In: *Computer Graphics Forum*. Vol. 39. 5. Wiley Online Library. 2020, pp. 197–207.

[Car+20a] Mathieu Carrière et al. “A note on stochastic subgradient descent for persistence-based functionals: convergence and practical aspects”. In: *arXiv preprint arXiv:2010.08356* (2020).

[Car+20b] Mathieu Carrière et al. “Perslay: A neural network layer for persistence diagrams and new graph topological signatures”. In: *International Conference on Artificial Intelligence and Statistics*. PMLR. 2020, pp. 2786–2796.

[CD20] Padraig Corcoran and Bailin Deng. “Regularization of Persistent Homology Gradient Computation”. In: *arXiv preprint arXiv:2011.05804* (2020).

[Dav+20] Damek Davis et al. “Stochastic subgradient method converges on tame functions”. In: *Foundations of computational mathematics* 20.1 (2020), pp. 119–154.

[Gab+20] Rickard Brüel Gabrielsson et al. “A topology layer for machine learning”. In: *International Conference on Artificial Intelligence and Statistics*. PMLR. 2020, pp. 1553–1563.

[Kac20] Oleg Kachan. “Persistent Homology-Based Projection Pursuit”. In: *Proceedings of the IEEE/CVF Conference on Computer Vision and Pattern Recognition Workshops*. 2020, pp. 856–857.

[SWB20] Elchanan Solomon, Alexander Wagner, and Paul Bendich. “A Fast and Robust Method for Global Topological Functional Optimization”. In: *arXiv preprint arXiv:2009.08496* (2020).

Appendix A. Differentiability of the extended persistence map

Let K be a finite simplicial complex with vertex set V and dimension $d \in \mathbb{N}$. A vertex function $f \in \mathbb{R}^V$ extends to the whole complex via $f(\sigma) := \max_{v \in \sigma} f(v)$. Filtrations, persistence modules and barcodes are then defined analogously to the case of a graph. The extended barcode of a function f now consists of $3(d+1)$ barcodes:

$$\text{EPH}(f) = \left[\{\text{EPH}_p^k(f)\}_{k \in \{\text{ord,ext,rel}\}} \right]_{p=0}^d \in \mathbf{Bar}^{3(d+1)}. \quad (26)$$

We then have the extended persistence map

$$\text{EPH} : \mathbb{R}^V \rightarrow \mathbf{Bar}^{3(d+1)},$$

and the ordinary persistence map as in remark 3.1

$$\text{PH} : f \in \mathbb{R}^K \longmapsto [\text{PH}_p(f)]_{p=0}^d \in \mathbf{Bar}^{d+1}.$$

Proposition A.1. Let K be a finite simplicial complex, and let $F : \mathcal{M} \rightarrow \mathbb{R}^V$ be a generically differentiable parametrisation. Then the composition $\text{EPH} \circ F$ is generically differentiable.

In particular, taking the parameter space \mathcal{M} to be the space \mathbb{R}^V of vertex functions, we obtain the generic differentiability of the extended persistence map EPH itself. Note that, however, we could not have directly deduced the generic differentiability of any composition of the form $\text{EPH} \circ F$ from the generic differentiability of EPH . This is due to the fact that the image of a parametrisation F might lie in the set where EPH is not differentiable.

The idea of our proof is to view the extended persistence of a vertex function $f \in \mathbb{R}^V$ as the ordinary persistence of an extension of f over the cone complex $\text{Cone}(K)$. We note that this point of view has proven to be particularly useful for computing extended persistence in practice [CEH09]. The relationship between EPH and PH can be described by a commutative diagram:

$$\begin{array}{ccc}
 \mathbb{R}^V & \xrightarrow{\text{EPH}} & \mathbf{Bar}^3 \\
 \downarrow & & \uparrow \\
 \mathbb{R}^{\text{Cone}(K)} & \xrightarrow{\text{PH}} & \mathbf{Bar}
 \end{array}$$

whose vertical maps are differentiable. Thus, we can deduce the differentiability of the extended persistence map EPH from the results of Leygonie, Oudot, and Tillmann [LOT19] about the ordinary persistence map PH .

PROOF OF PROPOSITION A.1. Let $f \in \mathbb{R}^V$ be a vertex function. Let K^t (resp. K_t) be the maximal subcomplexes of K induced by vertices taking values greater (resp less) than t . For $0 \leq p \leq d$, the associated p -th extended persistent homology module $V_p(f)$ is:

As such, $V_p(f)$ is a module indexed over the extended real line $\mathbb{R} \sqcup \{\infty\} \sqcup \mathbb{R}^{\text{op}}$. We construct an equivalent module $V_{p,R}(f)$ over the simpler, compact poset $[-R; 3R]$, where $R > 0$ is a large enough constant chosen hereafter. For this, we consider the poset map that collapses $\mathbb{R} \sqcup \{\infty\} \sqcup \mathbb{R}^{\text{op}}$ onto $[-R; 3R]$ as in fig. 3. Formally, the poset map is defined on \mathbb{R} as the canonical retraction onto $[-R; R]$, on \mathbb{R}^{op} as the symmetry $t \mapsto 2R - t$ followed by the canonical retraction onto $[-R; R]$, and sends the point ∞ to R .

If we choose $R > \sup_{\sigma} |f(\sigma)|$, then no new simplex enters the subcomplexes K_t or K^t for $t \notin [R; R]$ and $t \notin [R; R]^{\text{op}}$. Hence, the module $V_p(f)$ is locally constant outside of $[R; R]$ and $[R; R]^{\text{op}}$. By applying

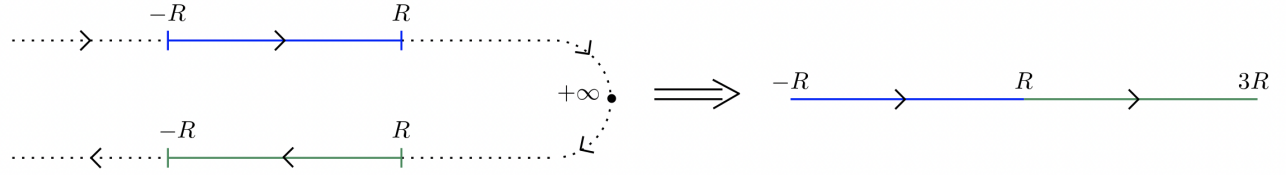


FIGURE 3. Collapsing the dotted part of the left poset yields the compact poset on the right.

the (inverse of the) poset map described above, we thus get a $[-R; 3R]$ -indexed module $V_{p,R}(f)$:

$$\begin{aligned}
 0 = H_p(K_{-R}) &\longrightarrow \cdots \longrightarrow H_p(K_s) \xrightarrow{s \leq t} H_p(K_t) \longrightarrow \cdots \longrightarrow H_p(K_R) \\
 0 = H_p(K, K^{-R}) &\leftarrow \cdots \leftarrow H_p(K, K^{2R-t}) \xleftarrow{t \geq s} H_p(K, K^{2R-s}) \leftarrow \cdots \leftarrow H_p(K; K^R)
 \end{aligned} \quad (28)$$

The extended module module $V_p(f)$ is essentially equivalent to the ordinary module $V_{p,R}(f)$, since we can retrieve the extended barcode $\text{EPH}_p(f)$ of $V_p(f)$ from the barcode of $V_{p,R}(f)$ as follows:

- Each interval $\langle b, d \rangle$ in the barcode of $V_{p,R}(f)$ such that $b \leq d < R$ yields an interval $\langle b, d \rangle$ in $\text{EPH}_p^{\text{ord}}(f)$;
- Each interval $\langle b, d \rangle$ in the barcode of $V_{p,R}(f)$ such that $b < R < d$ yields an interval $\langle b, 2R - d \rangle$ in $\text{EPH}_p^{\text{ext}}(f)$;
- Each interval $\langle b, d \rangle$ in the barcode of $V_{p,R}(f)$ such that $R < b \leq d$ yields an interval $\langle 2R - b, 2R - d \rangle$ in $\text{EPH}_p^{\text{rel}}(f)$.

We denote this decoding map by $\text{Dec}_R : \mathbf{Bar} \rightarrow \mathbf{Bar}^3$. We next take advantage of working with the ordinary module $V_{p,R}(f)$ by viewing it as the sub level set persistent homology module of a function defined on the cone $\text{Cone}(K)$.

Note that the relative homology groups of $V_{p,R}(f)$ in the second row of Eq. (28) may be replaced with ordinary (reduced) homology groups of the cones $\text{Cone}(K^{2R-t})$ using the functorial isomorphism:

$$H_p(K, K^{2R-t}) \cong \tilde{H}_p(K/K^{2R-t}) \cong \tilde{H}_p(K \cup \text{Cone}(K^{2R-t})).$$

We denote by ω the distinguished vertex of such cones. It is then clear that $V_{p,R}(f)$ equals the ordinary p -th sub level set persistent (reduced) homology module of the function $\hat{f}_R : \text{Cone}(K) \rightarrow \mathbb{R}$ defined by

$$\hat{f}_R(\sigma) := f(\sigma) \text{ and } \hat{f}_R(\sigma \sqcup \{\omega\}) := 2R - \min_{v \text{ vertex in } \sigma} f(v)$$

for any simplex $\sigma \in K$, and $\hat{f}_R(\omega) := -R$ by convention. Plugging these constructions together, we connect the ordinary and extended maps in the commutative diagram:³

$$\begin{array}{ccccc}
 & & \mathbb{R}^V & \xrightarrow{\text{EPH}} & \mathbf{Bar}^3 \\
 & \nearrow F & \downarrow f & & \uparrow \text{Dec}_R \\
 \mathcal{M} & \xrightarrow[\theta]{} & \mathbb{R}^{\text{Cone}(K)} & \xrightarrow{\text{PH}} & \mathbf{Bar} \\
 & \searrow & \hat{f}_R & & \\
 & & & &
 \end{array} \tag{29}$$

Note that this diagram only makes sense for parameters θ such that $F(\hat{\theta})_R$ is a function whose sub level sets are sub complexes of $\text{Cone}(K)$, as $\text{PH}(F(\hat{\theta})_R)$ is undefined otherwise. This requirement is satisfied whenever the inequality $\sup_{\sigma} |F(\hat{\theta})(\sigma)| < R$ holds. For simplicity, we assume that R can be chosen large enough for the inequality to hold for all parameters θ , hence the diagram (29) makes sense globally on \mathcal{M} . One can always avoid this restriction by working locally on compact neighbourhoods in \mathcal{M} .

From [LOT19, Theorem 4.9], the subset $\mathcal{M}' \subseteq \mathcal{M}$ where the parametrisation F is differentiable and induces a locally constant pre-order on simplices of K is a generic sub manifold. In turn, all the maps $\theta \mapsto \min_{v \in \sigma} F(\theta)(v)$ and $\theta \mapsto \max_{v \in \sigma} F(\theta)(v)$, for $\sigma \in K$ a simplex, are differentiable over \mathcal{M}' . Therefore $\hat{F}_R : \mathcal{M} \rightarrow \mathbb{R}^{\text{Cone}(K)}$ is differentiable over the generic submanifold \mathcal{M}' .

Since \hat{F}_R is generically differentiable, so is $\text{PH} \circ \hat{F}_R$ [LOT19, Theorem 4.9], i.e. we generically have local coordinate systems as in Def. 3.2. Since the decoding map Dec_R in diagram (29) merely applies an affine transformation to the local coordinate systems and then splits them into three parts (the splitting is constant), we obtain local coordinate systems for $\text{EPH} \circ F$. Therefore, $\text{EPH} \circ F$ is generically differentiable. \square

Appendix B. The wavelet signature is Well-defined

In definition 2.1, we defined the wavelet signature using the eigenvalues and eigenvectors of a graph Laplacian L . The wavelet signature is only well defined if it is independent of the choice of eigenbasis for L , where ambiguity could occur if L has eigenvalues with multiplicity⁴ greater than one.

Proposition 2.2. *The wavelet signature of a graph is independent of the choice of orthonormal eigenbasis for the Laplacian.*

PROOF. Let $\text{Spec}(L) \subset \mathbb{R}$ denote the spectrum of L and $\phi_1, \dots, \phi_{|V|}$ be a set of orthonormal eigenvectors of L . Let us denote $\Phi(\lambda)$ to be a $|V| \times m$ matrix where m corresponds to the geometric multiplicity

³Strictly speaking, the decoding map should furthermore forget the unique unbounded interval $(b, +\infty)$ in the barcode $\text{PH}(\hat{f}_R)$, since the ordinary persistence map PH computes the barcode of a module made of non-reduced homology groups.

⁴As L is symmetric and hence diagonalisable, the geometric and algebraic multiplicities of its eigenvalues agree.

of λ , and the m column vectors of $\Phi(\lambda)$ correspond to eigenvectors $\phi_{i_1}, \dots, \phi_{i_m}$ with eigenvalue λ . Then we can rewrite the wavelet signature eq. (3) as

$$W(g)_v = \sum_{i=1}^{|V|} g(\lambda_i) (\phi_i)_v^2 = \sum_{\lambda \in \text{Spec}(L)} g(\lambda) (\Phi(\lambda) \Phi(\lambda)^\top)_{vv} \quad (30)$$

Suppose we have another choice of eigenbasis of L . Without loss of generality for $\lambda \in \text{Spec}(L)$, the new basis $\phi'_{i_1}, \dots, \phi'_{i_m}$ for $\text{eig}(\lambda)$ is related to the previous eigenbasis $\phi_{i_1}, \dots, \phi_{i_m}$ by an orthonormal transformation transformation $U(\lambda) \in \mathbb{R}^{m \times m}$ on $\Phi(\lambda)$:

$$\Phi'(\lambda) = [\phi'_1 \ \cdots \ \phi'_m] = \Phi(\lambda)U(\lambda).$$

As $U(\lambda)$ is an orthonormal transformation with $U(\lambda)U(\lambda)^\top = 1$,

$$\begin{aligned} \Phi'(\lambda)\Phi'(\lambda)^\top &= \Phi(\lambda)U(\lambda)(\Phi(\lambda)U(\lambda))^\top \\ &= \Phi(\lambda)U(\lambda)U(\lambda)^\top\Phi(\lambda)^\top \\ &= \Phi(\lambda)\Phi(\lambda)^\top. \end{aligned}$$

Since the $V \times V$ matrix $\Phi(\lambda)\Phi(\lambda)^\top$ is independent of the choice of eigenbasis, the wavelet signature given on the right hand side of eq. (30) must also be independent of the choice of eigenbasis. \square

Appendix C. Experimental Implementation

As the graphs are all connected in the datasets we have chosen, the extended H_0 persistence diagram $\text{EPH}_0^{\text{ext}}$ consists of only one point. As such, we keep the extended and ordinary H_0 diagrams together as one H_0 diagram. Thus, we represent each graph as a set of three diagrams H_0 , $\text{EPH}_1^{\text{rel}}$ and $\text{EPH}_1^{\text{ext}}$ rather than four. Prior to vectorising the persistence diagrams, we apply a fixed, uniform affine transformation on the values of the vertex functions across all graphs such that the maximum and minimum values taken across all graphs in the dataset of the initial vertex functions before optimisation are scaled to 1 and 0 respectively. The diagrams for each graph are vectorised separately using and concatenated as a single vector.

Across all experiments, we use the Adam optimiser [KB14] with learning rate $\text{lr} = 1\text{e-}3$ to optimise the parameters of the neural network that takes the vectorised persistence diagrams as input. The wavelet parameters are updated using stochastic gradient descent with learning rate $\text{lr} = 1\text{e-}2$. The batch sizes for each experiment are shown in Table 4. In some experiments, we stop the optimisation of wavelet parameters at an early stopping epoch while the neural network parameters continue to be optimised. This is detailed in Table 5. We also describe how the wavelet parameters are initialised in Table 5.

C.1. Experiments described in Section 4.2.1 and Table 1. In these experiments, the three persistence diagrams of each graph are altogether converted into a vector in \mathbb{R}^{18} using Equation (25). The vectors are then classified by the sign of the output of the feed forward network

$$\text{FF} : \mathbb{R}^{18} \xrightarrow{\text{BN}} \mathbb{R}^{18} \xrightarrow{\text{Aff}} \mathbb{R} \quad (31)$$

where BN denotes a batch normalisation layer, and Aff denotes an affine transformation.

C.2. Experiments described in Section 4.2.2 and Table 2. In these experiments, the three persistence diagrams of each graph are altogether converted into a vector in \mathbb{R}^{18} using Equation (25). The vectors are then mapped to a classification ± 1 by a feed forward neural network with one hidden layer

$$\text{FF} : \mathbb{R}^{18} \xrightarrow{\text{BN}} \mathbb{R}^{18} \xrightarrow{\text{Aff}} \mathbb{R}^{18} \xrightarrow{\text{ReLU}} \mathbb{R}^{18} \xrightarrow{\text{BN}} \mathbb{R}^{18} \xrightarrow{\text{Aff}} \mathbb{R} \quad (32)$$

where the nonlinearity is $\text{ReLU}(x) = \max(x, 0)$. For MUTAG and COX2, we also insert a dropout layer [Sri+14] with dropout probability $p = 0.5$ before the final affine layer.

C.3. Experiments described in Section 4.2.3 and Table 3. For the experiments in Section 4.2.3, we vectorised each of the three persistence diagrams EPH_0 , $\text{EPH}_1^{\text{rel}}$ and $\text{EPH}_1^{\text{ext}}$ as a persistence image sampled on an 20×20 grid, whose grid points are equidistantly placed $\sigma = 1/17$ apart on the square $[-\sigma, 1 + \sigma]^2$ of the persistence diagrams, where σ is the width of the Gaussian. The Gaussian centred on the birth and persistence coordinates $\langle b, p \rangle$ of each point is weighted according to its persistence

$$\omega(p) = \sin^2\left(\frac{\pi}{2} \min\left(\frac{p}{\sigma}, 1\right)\right).$$

Points with persistence $p \geq \sigma$ are assigned a uniform weight $\omega = 1$, else assigned a weight that diminishes to zero as $p \rightarrow 0$. We then applied the following feed forward convolutional neural network to the persistence images:

$$\text{FF} : \mathbb{R}^{3 \times 20 \times 20} \xrightarrow{\text{BN2D}} \mathbb{R}^{3 \times 20 \times 20} \xrightarrow{\text{CNN}} \mathbb{R}^{15 \times 19 \times 19} \xrightarrow{\text{BN2D}} \mathbb{R}^{15 \times 19 \times 19} \xrightarrow{\text{CNN}} \mathbb{R}^{18 \times 18} \xrightarrow{\text{Aff}} \mathbb{R} \quad (33)$$

where CNN denotes a convolutional layer with kernel size 2, stride 1, followed by ReLU nonlinearity. The first CNN takes the three persistence images as three input channels and outputs fifteen channels. The final CNN combines these fifteen channels into a channel with one image.